ISSN 1392–1207. MECHANIKA. 2022 Volume 28(5): 358–363

Using the Stress Concentration Factor in Determining the Fracture Toughness

Goksel SARACOGLU
Faculty of Aeronautics and Astronautics, Iskenderun Technical University, 31200 Iskenderun, Hatay Türkiye,
E-mail: goksel.saracoglu@iste.edu.tr

crossref http://dx.doi.org/10.5755/j02.mech.31226

1. Introduction

In material fracture tests, the notch length and the artificial crack formed at the tip are theoretically specified as the crack length a. The stress concentration arising at the crack tip as a result of the applied stress causes fibre and matrix damage within and between the layers of the polymeric composite material [1, 2]. When the stress at the crack tip region reaches the effective fracture toughness of the material, uncontrolled fracture occurs in the material.

Many methodologies are used to estimate critical fracture toughness [3-5]. In the Internal Flaw Model (IFM), the stress concentration and hence damage region at the crack tip is defined as the energy-intensity region and the effect of this region is considered as the additional crack length [6]. The Point-Stress Criterion (PSC) states that the material will break if the stress value, which occurs after a certain characteristic distance d_0 from the crack tip, reaches the tensile strength σ_0 [7]. The methods based on the aforementioned critical distance have recently been discussed in detail [8].

Reaching the tensile strength after a certain distance from the crack tip means that a higher stress than tensile strength occurs at the crack tip. Therefore, it will be more meaningful to indicate that this (higher) value should be fracture toughness rather than stress. Establishing a relationship between the stress concentration at the crack tip and the stress intensity factor (SIF) would be meaningful approach in determining the critical fracture stress. Therefore, it is much more appropriate to consider tensile methods and fracture toughness together [9, 10]. In order to define the crack nucleation mechanism in the stress concentration region in brittle materials, theories have been put forward to use the energy and stress criteria in combination instead of applying them separately. In this case, the fracture toughness and geometry of the material come to the fore. In the combined method called finite fracture mechanics, the stress and energy flux acting through a small structural distance from the crack tip determine the fracture stress of the material [11-13].

In this study, by using the Irwin Equation in the load direction derived in the region close to the crack tip, a theoretical constant value was obtained for the crack tip radius in a three-point bending and tensile specimen with a single edge crack. This ensures that the components of the SIF are the crack-tip stress and the stress concentration factor (SCF) K_t. The fracture stresses of various crack length to width ratios a/W were determined using SCFs with theoretical radius and the obtained results were compared with the actual fracture stresses and the results of other methodologies.

2. The relationship between SIF and SCF

In Fig. 1, there is a hyperbolic notch in a part subjected to stress in both directions. The tip radius of curvature of the notch is ρ. The coordinate system starts inside the endpoint by $r = \rho/2$. When ρ/a (a half the two-tips crack length) is small compared to one, the origin is very close to the focal point of the ellipse or hyperbola representing the surface of the crack. This field equation in the load direction is similar to that for a "mathematically sharp" plane crack [14].

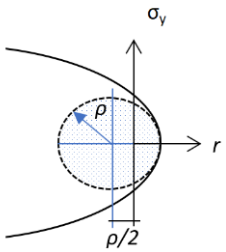

Fig. 1 Stress field coordinate system at hyperbolic notch tip [14]

The elastic stress distribution in the load direction adjacent to the elliptical holes and hyperbolic notches will be as in Eq. 1 [14]. The K_I and σ_y represents the Mode-I SIF and the stress in the load direction at the notch tip.

$$\sigma_y = \frac{K_I}{(2\pi r)^{1/2}} cos\frac{\theta}{2}\left[1 + sin\frac{\theta}{2} sin\frac{3\theta}{2}\right] + \\ + \frac{K_I}{(2\pi r)^{1/2}} \frac{\rho}{2r} cos\frac{3\theta}{2}. \quad (1)$$

$\theta = 0°$ and $r = \rho/2$ should be used for the maximum stress in the load direction at the crack tip:

$$\sigma_{max} = 2K_I / (\pi\rho)^{1/2}. \quad (2)$$

To include the SCF on the left side of Eq. 2, the maximum stress σ_{max} should be multiplied and divided by the nominal stress σ_n occured at the tip. To include only the SIF on the right-hand side of the equation, the notch tip radius ρ should theoretically have a value of 1.2732 mm. The SCF in which tip curvature is taken theoretically as ρ = 1.2732 mm acts as a stress multiplier K_I/σ in the SIF (Eq. (3)).

$$K_I = K_t \sigma_n, (\rho = 1.2732 \text{ mm}). \quad (3)$$

Thus, the maximum stress (in MPa) in the load direction to be encountered at the tip of the notch with a theoretical radius of 1.2732 mm will have the same value with the effective fracture toughness in terms of MPa.mm$^{1/2}$.

3. Three-point bending specimen

In a three-point bending specimen (TPB) with a critical fracture stress σ_f, the stress at the crack tip $\sigma_{f\text{-}a}$ will be $[W/(W\text{-}a)]^2\sigma_f$ at the end of the controlled fracture process (Fig. 2). The a and W represent the crack length and height, respectively. The end of controlled fracture will indicate that effective fracture toughness K_{eff} has been reached. The K_{eff} will be equal to the stress occurring at the crack tip multiplied by the SCF produced by the notch with the same crack length but with a tip radius of 1.2732 mm.

The K_{eff} determined for any crack size will also be valid for the others. Since the SCF values of all crack lengths based on ρ = 1.2732 mm will be calculated using Table 1 and Eq. (4), the critical stress will be found for any crack length.

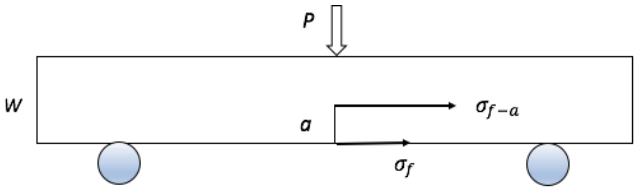

Fig. 2 Schematic view of TPB test specimen

Fig. 3 shows the bending specimen with an elliptical notch on one side. In Table 1, the relevant stress concentration factor components prepared according to the notch length a and radius of curvature ρ parameters are tabulated [15]. Eq. (4) shows the polynomial expression of the SCF with the a/W ratio of the components.

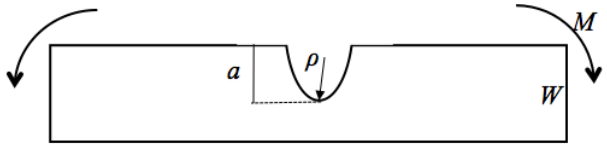

Fig. 3 Bending of a thin beam element [15]

$$K_t = C_1 + C_2\alpha + C_3\alpha^2 + C_4\alpha^3,\ (\alpha = a/W). \tag{4}$$

Table 1

SCF components of bending moment $\beta = a/\rho$ [15]

	$0.5 \le \beta \le 2$	$2 \le \beta \le 20$
C_1	$1.795+1.481\beta-0.211\beta^2$	$2.966+0.502\beta-0.009\beta^2$
C_2	$-3.544-3.677\beta+0.578\beta^2$	$-6.47-1.126\beta+0.019\beta^2$
C_3	$5.459+3.691\beta-0.565\beta^2$	$8.023+1.253\beta-0.020\beta^2$
C_4	$-2.678-1.531\beta+0.205\beta^2$	$-3.57-0.634\beta+0.010\beta^2$

4. Single edge-cracked tensile specimen

In the single edge-cracked tensile specimen (SENT), unlike the TPB, hybrid stress (tensile and bending) acts on the crack tip region and the effect of bending stress increases as the crack length increases. The SCF in the SENT may be considered as the superposition of the bending and tensile SCFs.

The SCFs for the bending and tensile stress components are calculated using Table 1 and Table 2, respectively. The Eq. (4) is also valid for the tensile SCF component. The theoretical value (1.2732 mm) is used for the tip radius ρ of the SCF components. Fig. 4 shows the tensile specimen with an elliptical notch on one side.

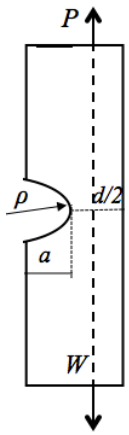

Fig. 4 Tensile loading in line with middle of ligament [15]

Table 2

SCF for loading in line with middle of ligament
$\beta = (a/\rho)^{1/2}$ [15]

	$0.5<\beta<2.0$	$2 < \beta < 20$
C_1	$0.907+2.15\beta-0.023\beta^2$	$0.953+2.136\beta-0.005\beta^2$
C_2	$0.710-11.289\beta+1.708\beta^2$	$-3.255-6.281\beta+0.068\beta^2$
C_3	$0.672+18.754\beta-4.046\beta^2$	$8.023+6.893\beta-0.064\beta^2$
C_4	$0.175-9.759\beta+2.365\beta^2$	$-4.851-2.793\beta+0.128\beta^2$

The SIF acting on the crack tip of the pin-loaded tensile specimen is found by Eq. (5):

$$K_I = \sigma_f\left[K_{t-tension} + \frac{3aW}{(W-a)^2}K_{t-bending}\right], \tag{5}$$

where: σ_f is the fracture stress of the specimen.

In Linear Elastic Fracture Mechanics, the SIF and the related geometric correction factor Y of the single edge-cracked tensile specimen is specified by Eqs. (6) and (7) [16], respectively $\alpha = a/W$:

$$K_I = \sigma_f Y(\pi a)^{1/2}, \tag{6}$$

$$Y = 1.12 - 0.231\alpha + 10.55\alpha^2 - 21.71\alpha^3 + 30.38\alpha^4,\ (\alpha \le 0.6). \tag{7}$$

Eqs. (5) and (6) will give the very close results at all crack lengths if the Eq. (5) is based on theoretical tip curvature 1.2732 mm as seen in Table 3. The both equations are for the pin-loaded condition where bending moment transfer is not restricted.

If Eqs. (6) and (7) are used for the clamped-end condition, the higher fracture stress obtained in this condition at a certain a/W crack length ratio will be multiplied by the higher the SCF produced by pin-loaded condition.

The geometric correction factors that should be used in the clamped-end condition for the SENT specimen are given in the first four columns of Table 4 [18-22]. In this case, the SCF in Eq. (5) needs to be compensated for the clamped-end condition.

Table 3

The comparison of the SCFs of Neuber's and photoelastic results with Eq.5 for the pin-loaded SENT

a/W	Neuber's [17]	Photoelastic [17]	This paper
0	1	-	
0.1	4.9		4.8
0.2	7.7	7.1	7.0
0.3	11		9.9
0.4	17	15	14.4
0.5	25	-	21.9
0.6	39	38	35.3
0.66	-	47	48.9
0.7	64	-	62.3
0.8	124	126	130

Table 4

The comparison of Y of clamped-end condition with $1.059Y^{1/2}$ for pin-loading

a/W	Blatt et al. [18]	Marchand et al. and Ahmed et al. [19, 20]	Dao and Mettu [21]	Bowie et al. [22]	This paper $1.059Y^{1/2}$
0.05	1.1228	1.14	1.1389	1.13	1.1385
0.1	1.1528	1.166	1.1581	1.16	1.1642
0.2	1.2411	1.251	1.2291	1.25	1.2442
0.3	1.3654	1.378	1.3604	1.37	1.3655
0.4	1.5147	1.539	1.5178	1.52	1.5370
0.5	1.6951	1.726	1.7029	1.70	1.7769
0.6	1.9026	1.934	1.9192	1.91	2.1240
0.7	2.1569	2.171	2.1801	2.17	
0.8	2.498	2.481	2.5322		
0.9	3.1502	3.113	3.1637		
0.95	4.0864	4.052	4.137		

If the geometric correction factor for the pin-load condition is used for clamped-end condition, it is possible to reach a constant SIF. The square of the SIF obtained at each a/W from Eq. (5) will reach a constant value when divided by the geometric correction factor of the related a/W (Eq. (8)). In other words, the strain energy release rate G_I needs to be normalized with Y, ($\alpha = a/W$):

$$\left[\frac{K_{eff}^2}{Y}\right]_{\alpha_1} = \left[\frac{K_{eff}^2}{Y}\right]_{\alpha_2} = \left[\frac{K_{eff}^2}{Y}\right]_{\alpha_n}. \quad (8)$$

Considering Eq. (8), using the geometric correction factor of pin-loading for the clamped-end condition, the classical SIF Equation in Linear Elastic Fracture Mechanics should be as seen Eq. (9):

$$K_I = \sigma_f \left(Y\pi a\right)^{1/2}. \quad (9)$$

In this case, Eq. (5) will have the form as seen in Eq. (10):

$$K_I = \frac{\sigma_f}{Y^{1/2}}\left[K_{t-tension} + \frac{3aW}{(W-a)^2}K_{t-bending}\right]. \quad (10)$$

The fifth column in Table 4 shows the values of $1.059Y^{1/2}$. It is seen that the values have a linear relationship up to $a/W \le 0.4$ crack length ratio.

Eq. (2), adapted for various crack length ratios, will take a form as seen in Eq. (11) at the limit of $a/W \to 0$. The σ_0 represents the tensile strength of the specimen:

$$K_Q = 1.12\sigma_0 \left(\pi\rho\right)^{1/2}, (\rho = 1.2732 \text{ mm}). \quad (11)$$

5. Model verification

Thornel 300 carbon fiber/epoxy $\left[0/90/\pm45\right]_{ns}$ laminated composite material, the results of which were examined in another study, is considered to ensure objectivity and to compare with other estimation methodologies [23]. The σ_0, E_{11}, E_{22} and υ_{12} are 581 MPa, 138 GPa, 11 GPa and 0.35, respectively. For the TPB, the span was 4.4 times the width W (W=25 mm) and for the clamped-end SENT, length L between jaws was 4.6 times the width W (W=40 mm).

In the TPB specimen, the experimental fracture stress at a/W = 0.24 was determined as σ_f = 269 MPa in its study (Table 5). The equivalent of this stress at the crack tip is calculated as $\sigma_{f\text{-}a}$ = 466 MPa. The SCF is calculated as a result of Table 1 which was used for ρ = 1.2732 mm and for the related crack length. The fracture toughness is calculated as 1440 MPa.mm$^{1/2}$. Dividing the obtained value by the SCFs for the other crack length ratios, using Table 1, will give the crack tip stress values $\sigma_{f\text{-}a}$ and after that the fracture stresses σ_f can be reached.

Table 5

The TPB critical fracture and crack tip stresses

a/W	K_t	σ_f, MPa	$\sigma_{f\text{-}a}$, MPa	$K_t\,\sigma_{f\text{-}a}$, MPa
0.24	3.094	269	466	1440
0.36	2.916	202	494	
0.48	2.708	144	532	
0.60	2.487	93	580	
0.72	2.212	51	652	

In Table 6, when the ratios of obtained fracture stresses to experimental values are examined, the error rate is 1.2 % at the most. It is seen that this rate is 4.5 % in DZM, 19 % in IFM and 9 % in PSC.

Table 6

The TPB test results comparison (in MPa)

a/W	Exp.	DZM	IFM c_0=1.64 mm	PSC d_0=0.63 mm	This paper
0.24	269	Ref.			
0.36	202	198	205	195	202
0.48	144	140	149	139	144
0.60	92	92	100	92	93
0.72	52	54	62	56	51

Fig. 5 shows the deviations in the ratio of the critical fracture stress to the tensile strength for the TPB specimen when different values are used for ρ. If the $a/W = 0.24$ ratio is chosen as a reference, it is seen that the error rate increases as the a/W ratio increases for $\rho = 0.636$ mm. If $\rho = 1.9092$ mm is used, it turns out that the error rates hover around the 0.0 % level as a sinusoidal wave, but the amplitude is higher than that of 1.2732 mm.

At the reference crack length ratio of $a/W = 0.20$, the experimental fracture stress was determined as 204 MPa in the SENT specimen in the study [23]. Using $\rho = 12732$ mm as a tip radius of curvature at the related crack lengths of a/W in both the bending and tensile specimen SCF tables (Table 1 and 2), the K_I is obtained as 1431 MPa.mm$^{1/2}$ in Eq. (5). Using Eq. (8), the SIFs for other a/Ws are found. If the found values are substituted in Eq. (5), the critical stress values σ_f are approximated. The constant K_{eff} is obtained by placing the found critical fracture stress in Eq. (10). It can be seen in Table 7 that K_{eff} is 1222 MPa.mm$^{1/2}$ for the sample under consideration.

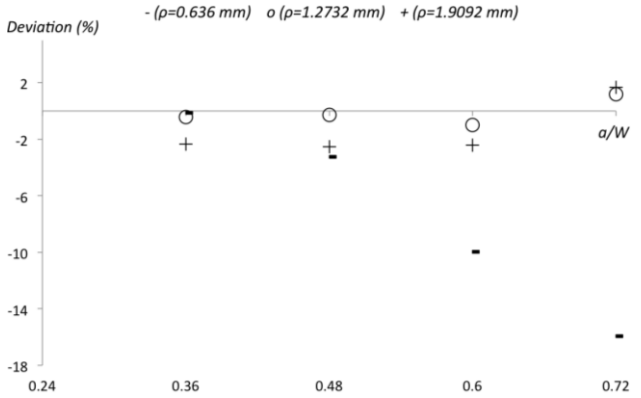

Fig. 5 The deviation results of different ρ values

Table 7

Obtaining constant effective fracture toughness in the SENT sample

a/W	K_I, Pa.mm$^{1/2}$ Eq. (8)	σ_f, MPa Eq. (5)	K_{eff}, MPa.mm$^{1/2}$ Eq.(10)
≈0.0	1294		1222
0.2	1431	204	
0.3	1574	150	
0.4	1771	116	
0.5	2052	94	
0.6	2444	69	

The graphical representation of K_I values obtained in the second column of Table 7 using Eq. (8) is given in Fig. 6. The decreasing curve towards the $a/W = 0$ limit is seen in the figure.

Table 8 includes the comparison of the fracture stress results of the tensile specimen between the other methodologies and the specified method in this paper. It is seen that the deviation rates of all methodologies from the experimental results increased compared to the TPB results. Considering that the variation between test samples is 8%, it can be considered that the closest results are obtained by the specified method in this paper and the DZM. The characteristic distances for IFM and PSC are the same as the values in Table 6.

Using Eq. (8), K_I was obtained as 1294 MPa.mm$^{1/2}$ for the $a/W \approx 0$ limit from the $a/W = 0.2$ (ref.) in Table 7. At the very small crack length ratio $a/W \approx 0$, the σ_0 tensile strength is determined as 577 MPa using Eq. (11), which is close to the experimental result 581 MPa.

If the experimentally obtained critical fracture stresses are replaced in Eq. (6), but the geometric correction factors in Table 4 are used, it is seen that the average K_{eff} values are close to 1222 MPa.mm$^{1/2}$ (Table 9).

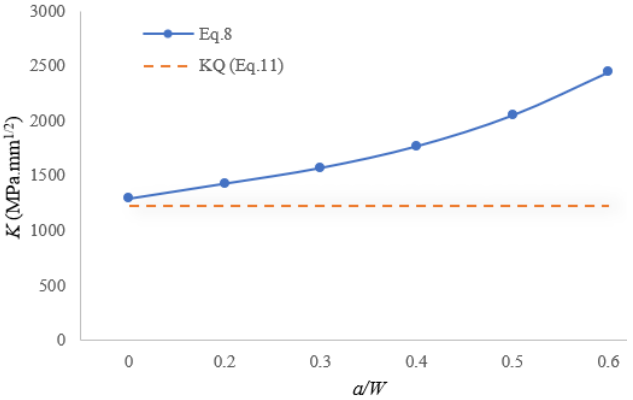

Fig. 6 The increasing mode of K_I due to pin-loaded geometric factor Y in the clamped-end condition

Table 8

Tensile test results comparison (in MPa)

a/W	Exp.	DZM	IFM	PSC	This paper Eq. (12)
0.2	204	223	175	169	204 (Ref.)
0.3	135	137	121	113	150
0.4	113	108	84	77	116
0.5	87	92	56	52	94
0.6	71	54	37	33	69

Table 9

Tensile test sample K_{eff} result comparison

a/W	Ref. [9]	Ref. [10, 11]	Ref. [12]	Ref. [13]
0.2	1269	1279	1257	1278
0.3	1130	1140	1126	1134
0.4	1214	1233	1216	1218
0.5	1171	1192	1176	1174
0.6	1171	1190	1181	1176
Avg.	**1191**	**1207**	**1191**	**1196**

6. Conclusions

It is seen that the SCF tables prepared for isotropic materials can give the critical fracture stresses and effective fracture toughness values of anisotropic materials close to the actual values. As in isotropic materials, it is seen that anisotropic materials have a constant fracture toughness value and when this value is reached, the material breaks. Roughly, the controlled crack propagation phase makes the difference.

In the stress distribution equation occurring in front of an elliptical cavity or notch, it has been stated that the critical fracture stress and SIF can be found by using the theoretical radius of curvature of the notch which provides the $\sigma_{max} = K_I$ at the stress concentration tables. Using

1.2732 mm to the tip radius of curvature in the SCF corresponds to the $Y(\pi a)^{1/2}$ value in the corresponding a/W ratio.

The fracture toughness values obtained in the three-point bending and the tensile tests are close to each other as they should be in the same material. The difference is due to that the bending specimen used for SCF data does not fully correspond to the three-point bending specimen.

The fracture stress results obtained from the model proposed in this paper are quite close to the experimental values in the three-point bending test and the deviation rates are lower than those of the DZM, IFM and the PSC methodologies. But, it is also seen that there is an increase in the deviation rates of the tensile test compared to the three-point bending test results. In this increase, the presence of tensile and bending stresses at the crack tip, which varies depending on the crack length ratio, is effective. However, when compared with the rates of other methodologies, it is seen that it can be applied successfully.

In order to use the SIF equation in Linear Elastic Fracture Mechanics in the tensile test results, the loading type should be considered. This study gives important results in terms of indicating that the increasing stress intensity factor of the pin-loaded tensile test with the geometric correction factor Y corresponds to a constant effective fracture toughness if normalization is made by using the geometric correction factor.

References

1. **Green, B. G.; Wisnom, M. R.; Hallett, S. R.** 2007. An experimental investigation into the tensile strength scaling of notched composites. Composites Part A: Applied Science and Manufacturing 38(3): 867e878. http://dx.doi.org/10.1016/j.compositesa.2006.07.00.
2. **Wisnom, M. R.; Hallett, S. R.; Soutis, C.** 2010. Scaling effects in notched composites. Journal of Composite Materials 44(2): 195e210. https://doi.org/10.1177/0021998309339865.
3. **Awerbuch, J.; Madhukar, M. S.** 1985. Notched Strength of Composite Laminates: Predictions and Experiments –A Review, Journal of Reinforced Plastics and Composites. https://doi.org/10.1177/073168448500400102.
4. **Papanicolaou, G. C.; Samoilis G.; Giannis S.; Barkoula N. M.; Karger-Kocsis, J.** 2002. A Model for the Accurate Prediction of the Residual Strength after Damage Due to Impact and Erosion of FRPs. In: Gdoutos E.E. (eds) Recent Advances in Experimental Mechanics. Springer, Dordrecht. https://doi.org/10.1007/0-306-48410-2_17.
5. **Potti, P. K.; Rao, B. N.; Srivastava, V. K.** 2001. Fracture strength of composite laminates containing surface notches, Advanced Composite Materials 10: 29 - 37. https://doi.org/10.1163/15685510152546349.
6. **Waddoups, M. E.; Eisenmann, J. R.; Kaminski, B. E.** 1971. Macroscopic fracture mechanics of advanced composite materials, Journal of Composite Materials 5: 446 - 454. https://doi.org/10.1177/002199837100500402.
7. **Whitney, J. M.; Nuismer, R. J.** 1974. Stress fracture criteria for laminated composites containing stress concentrations, Journal of Composite Materials 8: 253 - 265. https://doi.org/10.1177/002199837400800303.
8. **Taylor, D.** 2008. The theory of critical distances, Engineering Fracture Mechanics 75(7): 1696e1705.
9. **Soutis, C.; Fleck, N. A.** 1990. Static compression failure of carbon fibre T800/924C composite plate with a single hole, Journal of Composite Materials 24(5): 536–558. https://doi.org/10.1177/002199839002400505.
10. **Delprete, C.; Maggio, L.; Sesana, R.** 2021. Theory of critical distances: A discussion on concepts and applications, Proceedings of the Institution of Mechanical Engineers, Part C: Journal of Mechanical Engineering Science 235: 5695 - 5708. https://doi.org/10.1177/0954406220985887.
11. **Cornetti, P.; Pugno, N. M.; Carpinteri, A.; Taylor, D.** 2006. Finite fracture mechanics: a coupled stress and energy failure criterion, Engineering Fracture Mechanics 73: 2021-2033. https://doi.org/10.1016/j.engfracmech.2006.03.010.
12. **Rettl, M.; Pletz, M.; Schuecker, C.** 2022. Efficient prediction of crack initiation from arbitrary 2D notches, Theoretical and Applied Fracture Mechanics. https://doi.org/10.1016/j.tafmec.2022.103376.
13. **Martin, É.; Leguillon, D.; Carrère, N.** 2015. An extension of the point-stress criterion based on a coupled stress and energy fulfilment: Application to the prediction of the open-hole tensile strength of a composite plate. https://doi.org/10.1016/B978-0-08-100137-0.00017-1.
14. **Creager, M.; Paris, P.** 1967. Elastic field equations for blunt cracks with reference to stress corrosion cracking, International Journal of Fracture Mechanics 3: 247-252. https://doi.org/10.1007/BF00182890.
15. **Pilkey, W. D.; Pilkey, D. F.** 2008. Peterson's stress concentration factors. Third edition. John Wiley & Sons, Inc., Hoboken, New Jersey. https://doi.org/10.1002/9780470211106.
16. **Gross, B.; Srawley, J. E.; Brown, W. F.** 1964. Stress-intensity factors for a single-edge-notch tension specimen by boundary collocation of a stress function. Washington, D.C: National Aeronautics and Space Administration.
17. **Dixon, J. R.; Strannigan, J. S.; McGregor, J.** 1969. stress distribution in a tension specimen notched on one edge, J. Strain Anal. 4(1): 27–31. https://doi.org/10.1243/03093247V041027.
18. **Blatt, D.; John, R.; Coker, D.** 1994. Stress intensity factor and compliance solutions for a single edge notched specimen with clamped ends, Engineering Fracture Mechanics 47: 521-532. https://doi.org/10.1016/0013-7944(94)90252-6.
19. **Marchand, N. J.; Parks, D. M.; Pelloux, R. M.** 1986. K_I-solutions for single edge notch specimens under fixed end displacements, International Journal of Fracture 31: 53-65. https://doi.org/10.1007/BF00033929.
20. **Ahmad, J.; Papaspyropoulos, V.; Hopper, A.T.** 1991. Elastic-plastic analysis of edge-notched panels subjected to fixed grip loading, Engineering Fracture Mechanics 38: 283-294. https://doi.org/10.1016/0013-7944(91)90006-M.
21. **Dao, T. X.; Mettu, S. R.** 1991. Analysis of an edge-cracked specimen subjected to rotationally-constrained end displacements. NASA JSC 32171.

22. **Bowie, O. L.; Freese, C. E.; Neal, D. M.** 1973. Solution of plane problems of elasticity utilizing partitioning concepts, Journal of Applied Mechanics 40: 767-772. https://doi.org/10.1115/1.3423087.
23. **Aronsson, C.; Backlund, J. C.** 1986. Tensile fracture of laminates with cracks, Journal of Composite Materials 20: 287 - 307. https://doi.org/10.1177/002199838602000305.

G. Saracoglu

USING THE STRESS CONCENTRATION FACTOR IN DETERMINING THE FRACTURE TOUGHNESS

S u m m a r y

This paper offers the use of stress concentration factor in determining the critical fracture stress and fracture toughness of polymeric composite materials at various crack length ratios. The stress intensity factor has been turned into a function of the stress concentration factor derived from the maximum stress occurring at the notch tip and the tip stress generated by the force applied to the sample. This conversion allowed the use of a fixed theoretical radius 1.2732 mm instead of the actual radius of the notch or crack. On the edge cracked three-point bending and tensile samples, the specified method detects the three-point bending fracture stresses with a maximum error rate of 1.2 %. This study also establishes a relationship between the clamped end and the pin-loaded tensile specimens and states that the underlying mechanism of the stress intensity factor of the clamped end tensile specimen is based on the normalization of the stress intensity factor of the pin-loaded conditions with the geometric correction factor.

Keywords: fracture toughness, fracture stress prediction, stress concentration factor, stress intensity factor, edge-cracked sample.

Received April 21, 2022
Accepted October 17, 2022